Effect of Mo contents on corrosion and tribocorrosion behaviors of Ti-Mo alloys for orthopaedic implant application

Wei Xu [a, b †], Miao Chen [a †], Xin Lu [a *], Jingjing Tian [c], Harshpreet Singh [d], Chao Huang [a], Yu Yan [a], Xuanhui Qu [a], Chaozong Liu [b]

[a] Beijing Advanced Innovation Center for Materials Genome Engineering, Institute for Advanced Materials and Technology, University of Science and Technology Beijing, Beijing 100083, China

[b] John Scale Centre for Biomedical Engineering, University College London, Royal National Orthopaedic Hospital, Stanmore HA7 4LP, UK

[c] Central Laboratory, Peking Union Medical College Hospital, Peking Union Medical College and Chinese Academy of Medical Sciences, Beijing 100730, China

[d] Department of Chemical and Materials Engineering, University of Auckland, Private Bag 92019, Auckland 1142, New Zealand

Abstract

Ti-Mo alloys were fabricated via powder metallurgy (PM), and microstructure, corrosion and tribocorrosion ~~behaviors~~behaviours of the manufactured alloys were investigated. The microstructure of Ti-(8-16)_Mo alloy consisted of α and β phases while Ti-20Mo alloy only contained the β phase. With Mo content increased, the corrosion resistance of Ti-Mo alloys improved, and all Ti-Mo alloys showed better corrosion resistance than as-cast pure Ti and Ti-6Al-4V. The tribocorrosion resistance of Ti-Mo alloys enhanced firstly and then decreased slightly with Mo increase~~d~~. Ti-16Mo alloy presented highest tribocorrosion resistance. All these results suggest that PM-fabricated Ti-16Mo alloy is a

*** Corresponding author:** Xin Lu, Tel.: +86 10 6233 3981; E-mail address: luxin@ustb.edu.cn;

† **These authors contributed equally.**

promising material for bone-tissue applications.

Keywords

Ti-Mo alloys; microstructure; corrosion resistance; tribocorrosion behavior; orthopaedic implant materials.

1. Introduction

Because of low density, high specific strength, satisfying corrosion resistance, and excellent biocompatibility, Titanium (Ti) and its alloys are widely used as hard tissue implant materials in the field of orthopedic and dental [1-3]. However, currently used Ti and its alloys, such as Ti-6Al-7Nb, Ti-6Al-4V, and Ti-5Al-2.5Fe (wt.% hereafter), are at the risk of releasing toxic aluminum (Al) or vanadium (V) ions after long-term implantation *in vivo* [4]. The release of these ions in the human body may cause some diseases, such as Alzheimer's disease and mental disorders. Besides, the elastic modulus of these alloys (~110 GPa) is also higher than that of native human bone (0.01-30 GPa). The mismatch of the elastic modulus between the implant and the native human bone can cause stress shielding, which will result in bone resorption and hence lead to the failure of implanting finally [5]. Therefore, developing new Ti alloys with a lower elastic modulus and higher biocompatibility is an urgent demand for clinical application. Notable examples include Ti-13Nb-13Zr, Ti-12Mo-6Zr-2Fe, and Ti-15Mo alloys, which has been approved by the United States Food and Drug Administration (FDA). In particular, binary Ti-Mo alloys containing (8-20)_% Mo has attracted significant attention due to their reasonable cost, excellent mechanical properties,_ ~~and~~ corrosion resistance~~,~~ and low magnetic susceptibility [6-13].

As hard tissue implant materials, corrosion and tribocorrosion resistance of the materials are two crucial factors [14]. It has been reported that 20-30% of materials loss can be contributed to these two corrosion-related damage [15], and it produces a series of adverse effects. Such as, inducing the generation of debris in the human body, Which can ~~and the generated debris can be~~ accumulat~~c~~ion around the human tissues or become soluble in blood, which may lead to short-term adverse effects, e.g.~~,~~ inflammation and damage of cell tissue, ~~and long~~or long-term adverse effects, e.g.~~,~~ toxicity and

carcinogenetic response [16, 17]. Also, it can affect the releasing of metal ions, which is still one of the significant concerns related to the clinical aspects and the lifetime of the metallic implant materials [18]. Previous studies had demonstrated that the Ti-10Mo [19], Ti-12Mo [20], and Ti-20Mo [19] alloys exhibited higher corrosion resistance than as-cast pure Ti due to the passive protective film of TiO_2-MoO_3 formed on the surface of the alloys. However, a systematic study of the effect of Mo contents on the corrosion and tribocorrosion resistance of Ti-Mo alloys fabricated by powder metallurgy (PM) is still less comprehensive but is vital for its clinical applications.

In this paper, the effect of Mo content on corrosion and tribocorrosion behaviors of Ti-Mo alloys was systematically investigated using open-circuit potential (OCP), electrochemical impedance spectroscopy (EIS) and unidirectional sliding wear tests in phosphate-buffered saline (PBS) solution. In addition to establishing a necessary understanding of Mo effect on the corrosion and tribocorrosion performance of the PM-fabricated Ti-Mo alloys, it is hoped that this work will also provide insights into the corrosion and tribocorrosion mechanisms of Ti-Mo alloys, which can help the researcher further understand the synergistic phenomenon of Ti and its alloys.

Commented [BS1]: State what Mo is, only an abbreviation has been written

2. Materials and methods

2.1 Materials fabrication and characterization

In this study, Ti-Mo alloys containing different Mo content were fabricated from hydride-de-hydride (HDH) commercially pure titanium (Ti) powder and hydrogen-reduced molybdenum (Mo) powder (< 25 μm, 99.9%, Beijing Xin Rong Yuan Technology Co. Ltd, Beijing, China). The chemical compositions of the Ti and Mo powders are listed in Table 1. The Ti-Mo powder was mixed, cold-pressed into a cylindrical compact, and then sintered in the argon (Ar) protection environment at different temperatures. The detailed fabrication process was described in our previous

Commented [BS2]: Add to previous comment.

study [21-24].

Table 1. Chemical composition of Ti and Mo powders.

Powder	Chemical composition (wt.%)									
	H	C	N	O	Si	Cl	Fe	Ni	Ti	Mo
Ti	0.02	0.02	0.04	0.25	0.02	0.05	0.06	0	Bal.	0
Mo	0.07	0.05	0.05	0.20	0.02	0.01	0.06	0.01	0	Bal.

Phase constituents were identified by X-ray diffractometer (Rigaku) using Cu radiation. The microstructure of the alloys was observed by a scanning electron microscope (SEM, JSM-6480LV, Japan). Before microstructure observed, each specimen was ground with by abrasive paper, polished~~,~~ and then etched by Kroll's etchant. The composition of the Kroll's solution was as follows: hydrofluoric acid (5%), nitric acid (10%), and distilled water (85%).

2.2 Electrochemical tests

The corrosion resistance of Ti-Mo alloys with different Mo content added was tested using open-circuit potential (OCP), electrochemical impedance spectroscopy (EIS) in phosphate-buffered saline (PBS) solution according to ASTM G59-97 [25]. The composition of the PBS solution was as follows: NaCl 8 g/L, KCl 0.2 g/L, $KH_2PO_4 \cdot 0.2$ g/L, Na_2HPO_4 1.15 g/L, pH=7.2. For comparison, as-cast Ti6Al4V and pure Ti were studied simultaneously, which is commonly used in clinical applications as orthopedic and dental implants. All specimens were cut by electrical discharge machining (EDM) in a size of 10 mm (length) × 10 mm (width) × 2 mm (thickness). ~~And then T~~the specimens were sealed by epoxy resin with an exposed working surface of 1 cm^2 and were laser connected to copper (Cu) wire. Finally, specimens were ground with abrasive paper and ultrasonically cleaned with ethanol and distilled water for further use.

The corrosion resistance of each specimen was studied by the three-electrode system. The working electrode, reference electrode, and counter electrode were a specimen, saturated calomel electrode (SCE)~~,~~ and platinum foil, respectively. Before testing, the

specimen was immersed into the solution for 2h to stabilize the potential, ~~and~~ the corrosion potential vs. time curve was recorded continually. After that, the electrochemical impedance (Z) was measured in a frequency range from 10^5 Hz to 10^{-2} Hz. The obtained data were simulated by the simulation software (Zsimpwin). All experiments were repeated 5 times to verify the reproducibility.

2.3 Tribocorrosion tests

Tribocorrosion behaviors of Ti-Mo alloys with different Mo content added, as-cast Ti6Al4V and pure Ti were investigated by a ball-on-plate-tribometer (UMT-II) integrated with an electrochemical workstation. Specimens were cut by EDM in a size of 20 mm (length) × 6 mm (width) × 2 mm (thickness). All specimens were embedded in epoxy resin, and then ground, polished, ultrasonically cleaned and dried in vacuum.

Measuring of corrosion potential is selected as triboelectrochemical technique to study the tribocorrosion resistance of Ti-Mo alloys due to its simplicity for obtaining information on the surface state of the sliding metals [26]. A ~~T~~two electrode~~s~~ set up was employed, where the saturated calomel electrode (SCE) was the reference electrode, and the specimens were the working electrode with an exposed area of 120 mm^2. Open circuit potential (OCP) was measured before, during, and after sliding. Before sliding, each specimen was immersed in the solution for 2h to stable the potential. After the potential was stabled, the sliding action was initiated for 1 h. After that, the OCP values was recorded continually for another 0.5h. The equipment and sequences of OCP and sliding were shown in Fig. 1. The slip frequency was 1 Hz, and the stroke length was 15 mm. A zirconia ball with a diameter of 10 mm was used as the grinding material. All tests were carried out at room temperature with a load of 1.5 N. Coefficient of friction (COF) of each specimen was continuously recorded by the tester system during the wear tests. All experiments were repeated 5 times to verify the reproducibility.

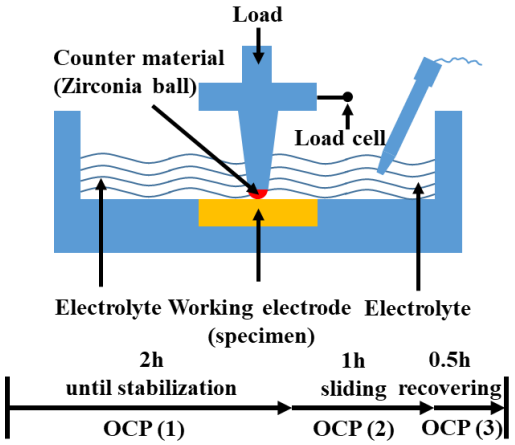

Fig. 1 Schematic view of the tribocorrosion experimental.

2.4 Surface characterization

After the tribocorrosion tests, specimens were ultrasonically cleaned in propanol for 10 min, followed by distilled water for 5 min, and worn surfaces were characterized using SEM (JSM-6480LV, Japan). The wear tracks were measured in terms of width and depth by white light interference microscope (Contour GTK, Bruker). Wear volume was calculated based on the pictures obtained by the white light interference microscope.

3. Results and discussion

3.1 Microstructure and hardness

Fig. 2 shows the XRD patterns of Ti-Mo alloys with different Mo contents added. It can be seen that all binary Ti-Mo alloys ~~were~~ consisted of mixed α and β phases except for Ti-20Mo alloy. This difference is caused by the β stabilizing action of Mo element [27]. When adding 8% and 10% Mo, the alloys were primarily composed of α phase with a small amount of β phase. With increasing Mo content, the volume fraction of β increased while that of the α phase decreased. When the Mo content added reached 16%, the formation of the α phase was suppressed significantly, and the alloy was dominated by β

phase with a small amount of α phase. Continuing to increase the Mo content to 20%, only the single β phase was observed.

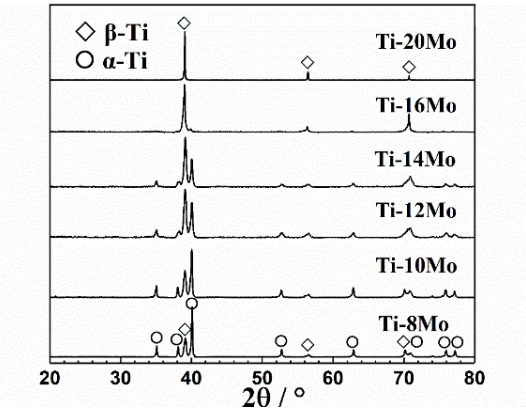

Fig. 2 XRD patterns of Ti-Mo alloys with different Mo contents added.

The SEM micrographs of Ti-Mo alloys with different Mo contents added are shown in Fig. 3. It can be seen that Ti-Mo alloys with high relative density and uniform microstructure can be obtained. Mo content has a strongly influenced on the microstructure of binary Ti-Mo alloys. As Fig. 3(a-e) shown, Ti-Mo alloys with Mo contents in the range of 8-16% exhibited similar microstructure, which consisted of the equiaxed grains of β phase and acicular of α phase. With continually increasing the Mo content to 20%, the Ti-Mo alloys were comprised of single β phase (Fig. 3(f)). These results were in accordance with the results of XRD. In addition, no distinct change in the size of β phase grains was observed in the case of specimens with different Mo contents added.

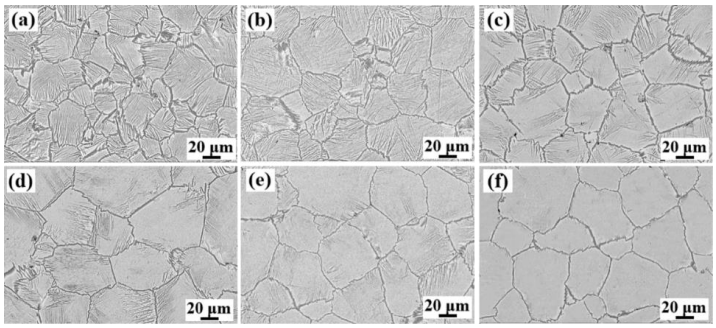

Fig. 3 SEM of Ti-Mo alloys with different Mo contents added.

The Micro-Vickers of Ti-Mo alloys with different Mo contents added are shown in Fig. 4. The hardness of Ti-Mo alloys showed a clear dependence on the Mo content, which increased gradually with the Mo content added and declined slightly afterward. The hardness of Ti-Mo alloys reached its maximum of 403 HV when ~~added~~ 16% Mo was added. This is mainly attributed to solid solution strengthening of Mo elements and precipitation strengthening of acicular α phase. With increasing Mo content, the solid solution strengthening effect was gradually enhanced, which leads to an improvement of the hardness. However, compared with Ti-16Mo alloy, Ti-20Mo alloy exhibited a lower value of hardness. This is mainly caused by the microstructure of the alloys. As discussed before, the Ti-16Mo alloy was dominated by β phase with a small amount of acicular α phase while the Ti-20Mo alloy was composed of a single β phase. It is believed that the small amount of acicular α phase in Ti-16Mo alloy can play the role of precipitation strengthening, which can improve the hardness of the alloy. This result is consistent with the findings of Majumdar et al. [18], who demonstrated that the acicular α phase was sandwiched between the β matrix within each packet and gave the local plastic constraints, leading to the strengthening of specimens. Compared with as-cast pure Ti and Ti-6Al-4V, all Ti-Mo alloys exhibited higher hardness than that of as-cast pure Ti and close to that of as-cast Ti-6Al-4V.

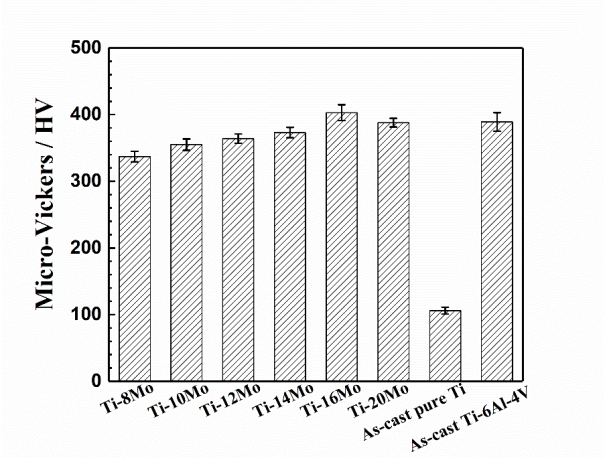

Fig. 4 Micro-Vickers of Ti-Mo alloys with different Mo contents added, as-cast pure Ti and as-cast Ti-6Al-4V.

3.2 Corrosion behavior

When the Ti and its alloys are implanted into the human body, they are surrounded by the body fluid containing mainly Na and Cl ions at 37 ℃ (310 K) [28]. This environment is much aggressive than the air or moisture environment. Hence, to simulate the environment, phosphate-buffered saline (PBS) solution at 37 ℃ was used in this study, which is often used as a testing solution to assess the corrosion resistance of Ti and its alloys in previous studies [29-31].

Commented [BS3]: More or less aggressive?

The evolution of open circuit potential (OCP) values of Ti-Mo alloys with different Mo contents added, as-cast pure Ti and as-cast Ti-6Al-4V during 2h of immersion in naturally aerated PBS solution at 37 ± 0.5 ℃ are shown in Fig. 5. All curves presented the same behaviors in PBS. With increasing the immersion time, E_{OCP} shifted towards positive direction at first, and then increased slowly and reached a quasi-stationary valve. With increasing the Mo content, the E_{OCP} values of Ti-Mo alloys exhibited a noble value, which indicated that the protective oxide film was more stable. Compared with the Ti-Mo alloys, as-cast pure Ti and as-cast Ti-6Al-4V shown a distinctly lower E_{OCP} values,

indicating that the oxide film formed on these alloys was less stable than that on Ti-Mo alloys.

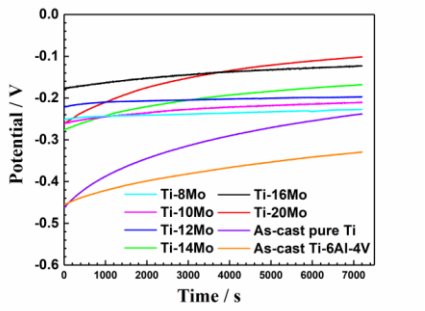

Fig. 5 Open-circuit potential (OCP) vs. time for Ti-Mo alloys with different Mo contents added, as-cast pure Ti and as-cast Ti-6Al-4V in naturally aerated PBS solution at 37 ± 0.5 °C.

Electrochemical impedance spectroscopy (EIS) measurements in naturally aerated PBS solution at 37 ± 0.5 °C are conducted further to obtain more electrochemical information. The results are expressed in Nyquist and Bode plots, as shown in Fig. 6. As Fig. 6(a) shown, all Nyquist plot were characterized by an incomplete and depressed semicircle, which indicates that a near capacitive response of passive film [32-34]. Also, with the Mo content increased the diameter of the capacitive loop increased gradually, meaning that the corrosion resistance of the alloys increased. Additionally, the Ti-Mo alloys with different Mo content added exhibited bigger dimeter of the capacitive loop than those of the as-cast pure Ti and Ti-6Al-4V, indicating that Ti-Mo alloys are more corrosion resistant.

The Bode plots, including impedance spectra and phase plots, are shown in Fig. 6(b). It can be seen that in the range of 10^3-10^5 Hz the slope of Bode impedance spectra was close to 0 and the negative phase angle dropped to near 0 degree, which is related to the response of electrolyte resistance. When the frequency was less than 10^3 Hz, all of the

Bode impedance spectra exhibited a slope of approximately -1, indicating a capacitive behavior's response of a passive film [32]. Besides, with increasing Mo content, the impedance modulus value of the Ti-Mo alloys increased gradually. For Bode phase plot, in moderate-frequency and low-frequency (less than 10^3 Hz) all specimens exhibited high negative phase angle (70-80°). Such phenomenon indicates that the formation of a passive film on the surface [35, 36]. With the Mo content increases, the alloys presented higher negative phase angle. These results indicate that with rising the Mo content, the corrosion resistance of the Ti-Mo alloys improved gradually, which is consistent with the results of OCP. Compared with as-cast pure Ti and Ti-6Al-4V, all of the Ti-Mo alloys exhibited higher impedance modulus value and negative phase angle, indicating higher corrosion resistance.

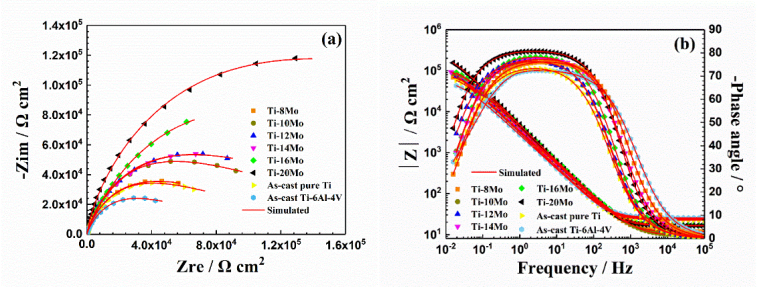

Fig. 6 (a) Nyquist and (b) Bode plots for Ti-Mo alloys with different Mo contents added, as-cast pure Ti and as-cast Ti-6Al-4V in naturally aerated PBS solution at 37 ± 0.5 °C compared with the simulation results.

In order to obtain more information on the oxide film formed on the surface of all alloys. The impedance spectra were fitted with the equivalent circuit. The equivalent circuit is shown in Fig. 7, which has been used in many Ti alloys to explain the change of the impedance with frequency [37-40]. In this circuit, R_s represents the electrolyte resistance, R_p and Q_b are associated with the rate of dissolution reaction and the ability of the charge transfer and with the film layer capacitance at the metal-electrolyte interface,

respectively.

The simulated curves and simulated impedance parameters are shown in Fig. 6 and Table 2, respectively. As Fig. 6 shown, the simulated values were consistent with the experimental values. Also, all of the chi-squared (χ^2) values all on the order of 10^{-4} (Table 2). These results indicate that a good fitting quality between the experimental EIS data and the proposed models was achieved. As Table 2 shown, with increasing the Mo content, the value of R_p and Q_b increased and decreased, respectively, which means that the corrosion resistance increased gradually. Compared with as-cast pure Ti and Ti-6Al-4V alloys, the Ti-Mo alloys exhibited higher R_p and lower Q_b, indicating that Ti-Mo alloys were more highly corrosion resistant than either the as-cast pure Ti or Ti6Al4V.

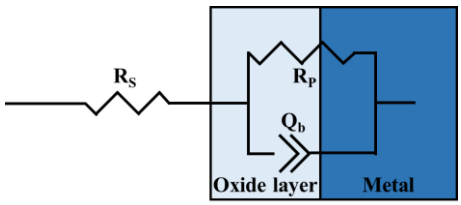

Fig. 7 Randle equivalent circuit for simulation results of impedance spectra of Ti-Mo alloys with different Mo contents added, as-cast pure Ti and as-cast Ti-6Al-4V in naturally aerated PBS solution at 37 ± 0.5 °C.

Table 2 Fitting parameters from EIS Ti-Mo alloys with different Mo contents added, as-cast pure Ti and as-cast Ti-6Al-4V in naturally aerated PBS solution at 37 ± 0.5 °C.

Alloys	R_s (Ω cm^2)	$Q_b \times 10^{-5}$ (F cm^{-2})	n_b	$R_p \times 10^5$ (Ω cm^2)	χ^2 (10^{-4})
Ti-8Mo	22.6 ± 1.7	5.1 ± 0.2	0.86 ± 0.11	0.88 ± 0.09	7.25 ± 0.15
Ti-10Mo	22.5 ± 2.1	4.7 ± 0.1	0.88 ± 0.12	1.21 ± 0.11	7.88 ± 0.21
Ti-12Mo	16.7 ± 1.5	4.3 ± 0.3	0.87 ± 0.21	1.32 ± 0.12	4.31 ± 0.36
Ti-14Mo	24.1 ± 1.6	4.1 ± 0.2	0.86 ± 0.19	1.35 ± 0.15	5.31 ± 0.18
Ti-16Mo	19.3 ± 1.9	3.8 ± 0.1	0.91 ± 0.17	2.44 ± 0.11	6.55 ± 0.25
Ti-20Mo	16.4 ± 1.4	3.5 ± 0.2	0.90 ± 0.21	2.74 ± 0.13	4.98 ± 0.19
As-cast pure Ti	21.6 ± 1.6	6.6 ± 0.4	0.88 ± 0.15	0.85 ± 0.15	4.58 ± 0.26
As-cast Ti-6Al-4V	25.3 ± 1.8	7.8 ± 0.4	0.93 ± 0.21	0.63 ± 0.08	5.22 ± 0.33

3.3 Tribocorrosion behavior

The evolution of open circuit potential (COP) before, during, and after sliding together with the coefficient of friction (COF) recorded during sliding in naturally aerated PBS solution at 37 ± 0.5 °C is presented in Fig. 8. It can be seen from Fig. 8(a) that COF of all alloys showed a similar tendency, which exhibited relatively steady-state behavior with few local fluctuations. With Mo content increased in the range of 8-20%, the values of COF decreased gradually and then increased slightly, indicating that the wear resistance of the Ti-Mo alloys improved at first and then decreased slightly. Compared with as-cast pure Ti and Ti-6Al-4V alloys, all of the Ti-Mo alloys exhibited lower COF values than that as-cast of pure Ti and close to that of Ti-6Al-4V, meaning that the wear resistance of Ti-Mo alloys is higher than as-cast pure Ti and close to as-cast Ti-6Al-4V alloy.

Regarding OCP evolution (Fig. 8(b)), the potential was stable for all of the Ti alloys before sliding. Then when sliding started, all samples presented an abrupt fall of the OCP, which is usually attributed to the damage of the formed passive film at the contact region due to the mechanical action [41, 42]. Under sliding, with increasing Mo content, the potential of Ti-Mo alloys shifted to positive position first and then to a negative position slightly. Among them, Ti-16Mo alloy presented the noblest potential, indicating that the lowest tendency for corrosion. Compared with as-cast pure Ti and Ti-6Al-4V alloys, all Ti-Mo alloys presented nobler potential than as-cast pure Ti but lower or close to than that of as-cast Ti-6Al-4V alloy, indicating that the tendency for corrosion of Ti-Mo alloys under sliding is lower than as-cast pure Ti but higher or close to than as-cast Ti-6Al-4V. Finally, when the mechanical contact stopped, OCP values recovered to higher values similar to those before sliding, indicating that repassivation phenomenon of the worn areas took place in all alloys to form new barriers against corrosion [43]. With Mo content increases the potential of Ti-Mo alloys increased firstly and then declined, indicating that

the repassivation capability was improved at first and then decreased. Similar to the results in sliding, the repassivation capability of Ti-Mo alloy was higher as-cast pure Ti but lower or close to than as-cast Ti-6Al-4V alloys.

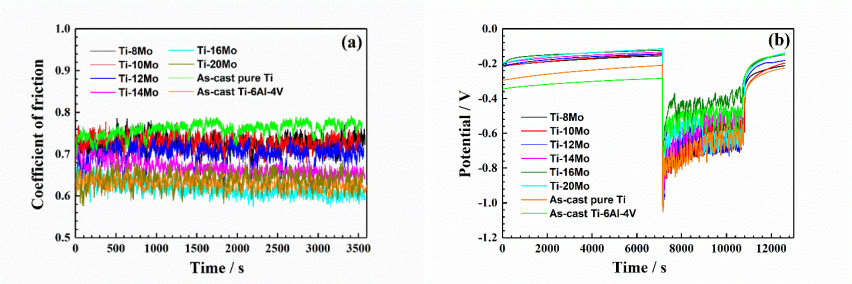

Fig. 8 Evolution of coefficient of friction (COF) (a) and open circuit potential (OCP) (b) of Ti-Mo alloys with different Mo contents added, as-cast pure Ti and as-cast Ti-6Al-4V during tribocorrosion test in naturally aerated PBS solution at 37 ± 0.5 °C.

To evaluate the tribocorrosion of the Ti-Mo alloys with different Mo content added further. The repassivation rate for a certain period was calculated by the formula (1), as follows:

$$\triangle E = K_1 \times \log t + K_2 \quad (1)$$

Where $\triangle E$ (V) is stated as the potential variation; t (s) is a certain period, which is usually 300 s after sliding; K_1 is repassivation rate; and K_2 is the constant, which is determined by the solution, and 0.1 for PBS. Fig. 9 shown the K_1 values for all of the Ti alloys. It can be seen that with Mo content increased the value of K_1 increased gradually, and when the Mo content reached 16 %, the value of K_1 reached the maximum. Continuing to increase the Mo content, the value of K_1 decreased slightly. This is mainly attributed to the Mo content and the hardness of the alloys. With Mo content increased, the passive layer of TiO_2-Mo_2O_3 was more stable, making it possible for the passive layer to stay longer and repassivate quickly [44]. Also, as discussed previously, the Ti-16Mo alloy exhibited the highest hardness, which results in the smallest damaged surface. Hence, the Ti-16Mo

alloy presented the highest K_1 value. Compared with the as-cast pure Ti and Ti-6Al-4V, the Ti-Mo alloys exhibited higher repassivation rate. This is mainly because the enthalpy formation of Mo with oxygen is much higher than that of other elements, such as V or Al, which can make them stay longer and repassivate quickly [2].

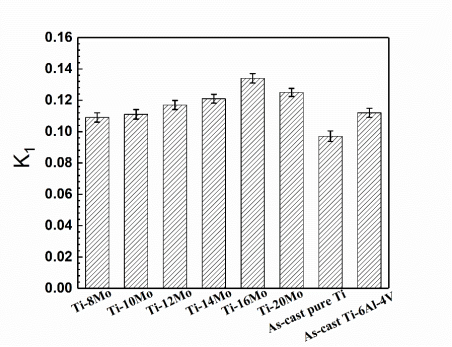

Fig. 9 Repassivation rate of Ti-Mo alloys with different Mo contents added, as-cast pure Ti and as-cast Ti-6Al-4V.

Wear tracks (a-h) and profiles (i) recorded on Ti-Mo alloys with different Mo contents added (a-f), as-cast pure Ti (g), and as-cast Ti-6Al-4V (h) after tribocorrosion test in naturally aerated PBS solution at 37 ± 0.5 °C, and wear volume (j) calculated from (i) are presented in Fig. 10. It can be seen from Fig. 10(a-h) that with Mo content increased, the wear track was much shallower and narrower. When the Mo content reached 16%, the wear tract was shallowest and narrowest, and continuing to increase the Mo content, the wear track became wider and deeper slightly. This result consists of the results of hardness. This result indicated that with the Mo content increased, the Ti-Mo alloys suffered smaller material removal. Compared with the as-cast pure Ti, all Ti-Mo alloys exhibited smaller wear, demonstrating the Ti-Mo alloys has higher wear resistance. Profiles and morphologies of the wear scars on Ti-Mo alloys with different Mo contents added, as-cast pure Ti, and as-cast Ti-6Al-4V and corresponding wear volume calculated from profiles are shown in Fig. 10 (i) and (j), respectively. It can be seen from Fig. 10 (j)

that with the Mo content increased the wear loss volume decreased gradually and then increased slightly, and the Ti-16Mo alloy has the lowest wear loss volume, which is consisted with results of hardness. Compared with as-cast pure Ti alloy, all of Ti-Mo alloys have lower wear loss volume than that of as-cast pure Ti alloy. As regarding the as-cast Ti-6Al-4V alloy, the wear loss volume is higher than Ti-16Mo alloy but lower than other Ti-Mo alloys. The differences in wear rate are associated with the hardness of the specimens. It has been demonstrated that an improvement in the hardness of alloys can enhance their wear resistance [45]. In this study, the Ti-Mo and Ti6Al4V alloys showed greater hardness than the pure Ti, and hence, both of these displayed lower wear rates than the pure Ti.

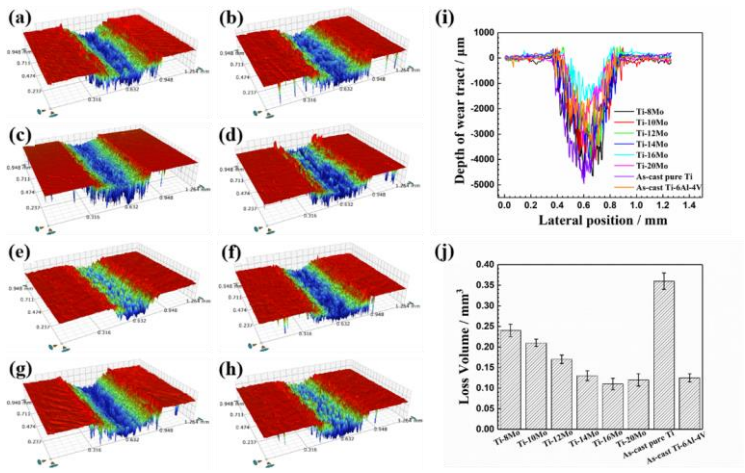

Fig. 10 (a-h) 3D surface profilometry and (i) recorded on Ti-Mo alloys with different Mo contents added (a-f), as-cast pure Ti (g), and as-cast Ti-6Al-4V (h)after tribocorrosion test in naturally aerated PBS solution at 37 ± 0.5 °C, and (j) wear volume calculated from (i).

The morphologies of the worn surfaces generated taken from the center of the wear tracks representing the worn areas after tribocorrosion tests are shown in Fig. 11. It can be seen from SE images that all of the Ti alloys showed evidence of grooves parallel to

the sliding direction, which demonstrated that the abrasive wear occurred. With the Mo content increased, the grooves observed were much shallower. This is mainly because of the increased hardness of the alloys, which agrees with the results of COF observed before. From BSE images, it can be seen that two different areas, e.g., dark and grey zones, are existed in all of the Ti alloys. Take the Ti-14Mo alloy, for example (Fig. 11(d)), two different areas Z1 and Z2, corresponding to grey and dark zones were observed. Based on the EDS results (Fig. 11(i)), the area of Z1 mainly consisted of Ti and Mo elements while Z2 had Ti, Mo, and O elements. This showed oxygen only in the dark area (Z2), meaning that these regions consisted of oxides, probably TiO_2 and MoO_3 [46]. The repetitive transfer between the sliding surfaces and its oxidation leads to the formation of oxidized wear debris and eventually their adhesion to the surface. As for as-cast pure Ti and Ti-6Al-4V alloys, similar to the surface of Ti-14Mo alloy, the oxygen only existed in the dark area (Fig. 11(g) Z4 and (h) Z6). Based on the EDS results (Fig. 11(i)), the composition of dark zones consisted of Ti and O elements, and Ti, O, and Al elements, respectively, which indicates that the oxides consisted of TiO_2 and TiO_2- Al_2O_3, respectively. Also, it was worth noticing that there is more oxide in the pure Ti alloy than Ti-6Al-4V and Ti-14Mo alloys, which could be related to the higher COF values during sliding. Because the higher amount of oxide can lead to the COF increase (Fig. 8(a)). As a result, the wear mechanisms under synergistic interactions between wear and corrosion for all the alloy were shown as a combination of abrasion and adhesive by the presence of grooves and some adhesive oxide, respectively.

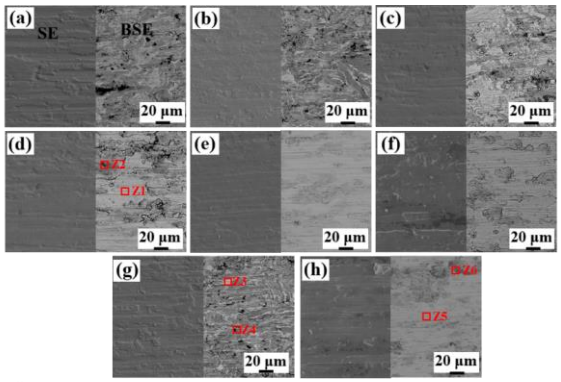

(i)

Materials	Marked areas	Ti(wt.%)	Mo(wt.%)	O(wt.%)	Al(wt.%)	V(wt.%)
Ti-14Mo	Z1	85.68	14.32	0	-	-
	Z2	74.15	12.29	13.56	-	-
Pure Ti	Z3	100	-	0	-	-
	Z4	76.23	-	23.77	-	-
Ti-6Al-4V	Z5	89.16	-	0	5.91	4.93
	Z6	77.76	-	11.63	6.14	4.47

Fig. 11 Detailed back-scattered electron and secondary electron (BSE-SE) images of the worn surfaces after tribocorrosion test of Ti-Mo alloys with different Mo contents added (a) 8%; (b) 10%; (c) 12%; (d) 14%; (e) 16%; (f) 20%, as-cast pure Ti (g), as-cast Ti-6Al-4V (h), and EDS analysis taken from the marked areas (i).

4. Conclusions

(1) Ti-Mo alloys with uniform microstructure and high relative density were fabricated by powder metallurgy (PM). The Ti-(8-16)Mo alloys consisted of acicular α phase surrounded by equiaxed grains of β phase while the Ti-20Mo alloy only contained a single β phase. With Mo content increased, the hardness of the alloys increased gradually at first and declined slightly afterward, and the Ti-16Mo alloy exhibited the highest hardness with 403 HV.

(2) The PM-fabricated Ti-Mo alloys exhibited spontaneous passivity in PBS solution. With Mo content increased, the Ti-Mo alloy showed higher corrosion resistance, including nobler E_{OCP}, higher $R_{p,}$ and lower Q_b. Compared with as-cast pure Ti and Ti-6Al-4V alloys, all Ti-Mo presented higher corrosion resistance.

(3) With Mo content increased, the tribocorrosion resistance of Ti-Mo alloys increased firstly and then decreased slightly. The Ti-16Mo alloy exhibited the highest repassivation rate with K_1 of 0.134, and lowest wear loss volume of 0.11 mm^3. The wear mechanisms under synergistic interactions between wear and corrosion for all the surfaces were shown as a combination of abrasion and adhesive.

(4) The highest tribocorrosion resistance, together with the satisfying corrosion resistance and easy net-shape manufacturability makes PM-fabricated Ti-16Mo alloy an attractive candidate for bone-tissue applications.

Acknowledgments

This research work is supported by the National Natural Science Foundation of China (51874037), 13th Five-Year Weapons Innovation Foundation of China (6141B012807) and State Key Lab of Advanced Metals and Materials, University of Science and Technology Beijing (2019-Z14). Cuie Wen acknowledges the financial support for this research by the National Health and Medical Research Council (NHMRC), Australia through project grant (GNT1087290). Wei Xu acknowledges the support from the China Scholarship Council (CSC) for a CSC Ph.D. scholarship (201906460106).

Data availability

The data that support the findings of this study are available from the corresponding authors on reasonable request.

Conflict of interest

The authors declare that they have no known competing for financial interests or personal relationships that could have appeared to influence the work reported in this paper.

References

[1] A. Nouri, C. Wen, 1-Introduction to surface coating and modification for metallic biomaterials, in: surface coating and modification of metallic biomaterials, Woodhead Publishing, 2015, pp. 3-60.

[2] M. Geetha, A.K. Singh, R. Asokamani, A.K. Gogia, Ti based biomaterials, the ultimate choice for orthopaedic implants-A review, Prog. Mater. Sci. 54 (2009) 397-425.

[3] M. Niinomi, M. Nakai, J. Hieda, Development of new metallic alloys for biomedical applications, Acta Biomater. 8 (2012) 3888-3903.

[4] H. Kröger, P. Venesmaa, J. Jurvelin, H. Miettinen, O. Suomalainen, E. Alhava, Bone density at the proximal femur after total hip arthroplasty, Clin. Orthop. Relat. R. 352 (1998) 66-74.

[5] B. Aksakal, O.S. Yildirim, H. Gul, Metallurgical failure analysis of various implant materials used in orthopedic applications, J. Fail. Anal. Prev. 4 (2004) 17-23.

[6] W.F. Ho, C.P. Ju, J.C. Lin, Structure and properties of cast binary Ti-Mo alloys, Biomaterials 20 (1999) 2115-2122.

[7] W. Xu, Z. Liu, X. Lu, J.J. Tian, G. Chen, B.W. Liu, Z. Li, X.H. Qu, C.E. Wen, Porous Ti-10Mo alloy fabricated by powder metallurgy for promoting bone regeneration, Sci. China Mater. 62 (2019) 1053-1064.

[8] N.T.C. Oliveira, A.C. Guastaldi, Electrochemical stability and corrosion resistance of Ti-Mo alloys for biomedical applications, Acta Biomater. 5 (2009) 399-405.

[9] J. Disegi, Wrought Titanium-15% molybdenum implant material, SYNTHES® Instruments and Implants, Second Edition, April 2009.

[10] W. Xu, X. Lu, B. Zhang, C.C. Liu, S.M. Lv, S.D. Yang, X.H. Qu, Effects of porosity on mechanical properties and corrosion resistances of PM-fabricated porous Ti-

426 10Mo alloy, Metals 8 (2018) 188-201.
427 [11] ATI 15Mo^{TM} Titanium alloy technical data sheet, ATI Allvac, Monroe, NC.
428 [12] V.R. Jablokov, M.J. Nutt, M.E. Richelsoph, H.L Freese, The application of Ti-15Mo
429 beta titanium alloy in high strength structural orthopaedic applications, J. ASTM Int.
430 2 (2005) 1-8.
431 [13] J.H. Lin, C.P. Ju, W.F. Ho, inventors, J.H. Chern, assignee, Biocompatible low
432 modulus titanium alloy for medical implant, United States patent (6409852) 2002
433 Jun. 25.
434 [14] C.E.B. Marino, L.H. Mascaro, EIS characterization of a Ti-dental implant in
435 artificial saliva media: dissolution process of the oxide barrier, J. Electroanal. Chem.
436 568 (2004) 115-120.
437 [15] Y. Yan, A. Neville, D. Dowson, Biotribocorrosion-an appraisal of the time
438 dependence of wear and corrosion interactions: I. The role of corrosion, J. Phys. D.
439 Appl. Phys. 39 (2006) 3200-3205.
440 [16] L. Kunčická, R. Kocich, T.C. Lowe, Advances in metals and alloys for joint
441 replacement, Prog. Mater. Sci. 88 (2017) 232-280.
442 [17] M. Hussein, A. Mohammed, N. Al-Aqeeli, Wear characteristics of metallic
443 biomaterials: a review, Materials 8 (2015) 2749-2768.
444 [18] A. Sargeant, T. Goswami, Hip implants-Paper VI - ion concentrations, Mater. Des.
445 28 (2007) 155-171.
446 [19] Y.L. Zhou, D. M. Luo, Corrosion behavior of Ti-Mo alloys cold rolled and heat
447 treated, J. Alloy. Compd. 509 (2011) 6267-6272.
448 [20] W. Xu, X. Lu, L.N. Wang, Z.M. Shi, S.M. Lv, Q. Ma, X.H. Qu, Mechanical
449 properties, in vitro corrosion resistance and biocompatibility of metal injection
450 molded Ti-12Mo alloy for dental applications, J. Mech. Behav. Biomed. 88 (2018)

534-547

[21] Y.W. Lin, X. Lu, B. Sun, C.C. Liu, X.H. Qu, Microstructure and mechanical properties of Ti-Mo alloys by powder metallurgy process, Rare Metal. Mater. Eng. 46 (2017) 1387-1392.

[22] W. Xu, M. Li, C.E. Wen, S.M. Lv, C.C. Liu, X. Lu, X.H. Qu, The mechanical properties and in vitro biocompatibility of pm-fabricated Ti-28Nb-35.Zr alloy for orthopedic implant applications, Materials 11 (2018) 531-543.

[23] W. Xu, S.Q. Xiao, X. Lu, G. Chen, C.C. Liu, X.H. Qu, Fabrication of commercial pure Ti by selective laser melting using hydride-dehydride titanium powders treated by ball milling, J. Mater. Sci. Technol. 35 (2019) 322-327.

[24] W. Xu, X. Lu, M.D. Hayat, J.J. Tian, C. Huang, M. Chen, X.H. Qu, C.E Wen, Pore characteristics, mechanical properties, and corrosion resistance of newly developed porous Ti35Zr28Nb scaffolds fabricated by powder metallurgy for bone-tissue engineering, J. Mater. Res. Technol. doi.org/10.1016/j.jmrt.2019.06.021

[25] ASTM G59-97, Standard test method for conducting potentiodynamic polarization resistance measurements, West Conshohocken, PA: ASTM International, 2014.

[26] S. Mischler, Triboelectrochemical techniques and interpretation methods in tribocorrosion: a comparative evaluation, Tribol. Int. 41 (2008) 573-583.

[27] D. Banerjee, J.C. Williams, Perspectives on Titanium Science and Technology, Acta Mater. 61 (2013) 844-879.

[28] T. P. Hoar, D. C. Mears, U. R. Evans, Corrosion-resistant alloys in chloride solution: materials for surgical implants, Proc. Roy. Soc. A, 294 (1966), 486-510.

[29] Y. Bai, X. Gai, S.J. L.C. Zhang, Y.J. Liu, Y.L. Hao, X. Zhang, R. Yang, Y.B. Gao, Improved corrosion behaviour of electron beam melted Ti-6Al-V alloy in phosphate buffered saline, Corros. Sci. 123 (2017) 289-296.

476 [30] T.M. Manhabosco, S.M. Tamborim, C.B. dos Santos, I.L. Müller, Tribological,
477 electrochemical and tribo-electrochemical characterization of bare and nitrided
478 Ti6Al4V in simulated body fluid solution, Corros. Sci. 53 (2011) 1786-1793.
479 [31] R. Yazdi, H.M. Ghasemi, C. Wang, A. Neville, Bio-corrosion behaviour of oxygen
480 diffusion layer on Ti-6Al-4V during tribocorrosion, Corros. Sci. 128 (2017) 23-32.
481 [32] Y. Bai, S.J. Li, F. Prima, Y.L. Hao, R. Yang, Electrochemical corrosion behavior of
482 Ti-24Nb-4Zr-8Sn alloy in a simulated physiological environment, Appl. Surf. Sci.
483 258 (2012) 4035-4040.
484 [33] W.R. Osório, A. Cremasco, P.N. Andrade, A. Garcia, R. Caram, Electrochemical
485 behavior of centrifuged cast and heat treated Ti-Cu alloys for medical applications,
486 Electrochim. Acta 55 (2010) 759-770.
487 [34] C. Vasilescu, S.I. Drob, E.I. Neacsu, J.C. Mirza Rosca, Surface analysis and
488 corrosion resistance of a new titanium base alloy in simulated body fluids, Corros.
489 Sci. 65 (2012) 431-440.
490 [35] A.W.E. Hodgson, Y. Mueller, D.C. Forster, S. Virtanen, Electrochemical
491 characterisation of passive films on Ti alloys under simulated biological conditions,
492 Electrochim. Acta 47 (2002) 1913-1923.
493 [36] F. Rosalbino, D. Maccio, G. Scavino, A. Saccone, In vitro corrosion behaviour of
494 Ti-Nb-Sn shape memory alloys in Ringer's physiological solution, J. Mater. Sci.:
495 Mater. M. 23 (2012) 865-871.
496 [37] B.L. Wang, Y.F. Zheng, L.C. Zhao, Effects of Hf content and immersion time on
497 electrochemical behavior of biomedical Ti-22Nb-xHf alloys in 0.9% NaCl solution,
498 Mater. Corros. 60 (2009) 330-335.
499 [38] X. Cheng, S.G. Roscoe, Corrosion behavior of titanium in the presence of calcium
500 phosphate and serum proteins, Biomaterials 26 (2005) 7350-7356.

[39] S. Tamilselvi, N. Rajendran, Electrochemical studies on the stability and corrosion resistance of Ti-5Al-2Nb-1Ta alloy for biomedical applications, Trends Biomaterials Artif. Organs 20 (2006) 49-52.

[40] I.C. Lavos-Valereto, S. Wolynec, I. Ramires, A.C. Guastaldi, I. Costa, Electrochemical impedance spectroscopy characterization of passive film formed on implant Ti-6Al-7Nb alloy in Hank's solution, J. Mater. Sci. Mater. M. 15 (2004) 55-59.

[41] Z. Doni, A.C. Alves, F. Toptan, J.R. Gomes, A. Ramalho, M. Buciumeanu, L. Palaghian, F.S. Silva, Dry sliding and tribocorrosion behaviour of hot pressed CoCrMo biomedical alloy as compared with the cast CoCrMo and Ti6Al4V alloys, Mater. Des. 52 (2013) 47-57.

[42] J. Chen, F.Y. Yan, B.B. Chen, J.Z. Wang, Assessing the tribocorrosion performance of Ti-6Al-4V, 316 stainless steel and Monel K500 alloys in artificial seawater, Mater. Corros. 64 (2013) 394-401.

[43] Z. Doni, A.C. Alves, F. Toptan, L.A. Rocha, M. Buciumeanu, Tribocorrosion behavior of hot pressed CoCrMo-HAP biocomposites, Tribol. Int. 91 (2015) 221-227.

[44] N.T.C. Oliveira, A.C. Guastaldi, Electrochemical behavior of Ti-Mo alloys applied as biomaterial, Corros. Sci. 50 (2008) 431-440.

[45] F. Movassagh-Alanagh, A. Abdollah-Zadeh, M. Aliofkhazraei, M. Abedi, Improving the wear and corrosion resistance of Ti-6Al-4V alloy by deposition of TiSiN nanocomposite coating with pulsed-DC PACVD, Wear 390-391 (2017) 93-103.

[46] A.F. Yetim. Investigation of wear behavior of titanium oxide films, produced by anodic oxidation, on commercially pure titanium in vacuum conditions, Surface &

526 Coatings Technology 205 (2010) 1757-1763.